Toxicology 482 (2022) 153370

Contents lists available at ScienceDirect

Toxicology

journal homepage: www.elsevier.com/locate/toxicol

Phytosphingosine-induced cell apoptosis via a mitochondrially mediated pathway

Jiaojiao Li [a,1], Jiayao Wen [a,1], Chunxiao Sun [a], Yuan Zhou [a], Jun Xu [a], Hugh J. MacIsaac [b], Xuexiu Chang [c,*], Qinghua Cui [d,*]

[a] School of Ecology and Environmental Science, Yunnan University, Kunming 650091, PR China
[b] Great Lakes Institute for Environmental Research, University of Windsor, Windsor, ON N9B 3P4, Canada
[c] College of Agronomy and Life Sciences, Kunming University, Kunming 650214, PR China
[d] School of Life Sciences, Yunnan University, Kunming 650091, PR China

ARTICLE INFO

Handling Editor: Dr. Mathieu Vinken

Keywords:
Microcystis aeruginosa
Exudate
Nasopharyngeal carcinoma cell
Mitophagy
Ca^{2+} overload
Cyanobacterial bloom

ABSTRACT

Cyanobacterial blooms, usually dominated by *Microcystis aeruginosa*, pose a serious threat to global freshwater ecosystems owing to their production and release of various harmful secondary metabolites. Detection of the chemicals in *M. aeruginosa* exudates using metabolomics technology revealed that phytosphingosine (PHS) was one of the most abundant compounds. However, its specific toxicological mechanism remained unclear. CNE-2 cells were selected to illustrate the cytotoxic mechanism of PHS, and it was determined to cause excessive production of reactive oxygen species and subsequently damage the mitochondrial structure. Mitochondrial membrane rupture led to matrix mitochondrial membrane potential disintegration, which induced Ca^{2+} overload and interrupted ATP synthesis. Furthermore, rupture of the mitochondrial membrane induced the opening of the permeability transition pore, which caused the release of proapoptotic factors into the cytoplasm and the expression of apoptosis-related proteins Bax, Bcl-2, cytochrome-c and cleaved caspase-3 in CNE-2 cells. These events, in turn, activated the mitochondrially mediated intrinsic apoptotic pathway. A mitochondrial repair mechanism, namely, PINK1/Parkin-mediated mitophagy, was then blocked, which further promoted apoptosis. Our findings suggest that more attention should be paid to the ecotoxicity of PHS, which is already listed as a contaminant of emerging concern.

1. Introduction

Cyanobacterial harmful algal blooms (cHABs) are a serious problem globally, largely owing to the harmful, secondary metabolites that they produce and release upon cell lysis (Janssen, 2019; Jones et al., 2021). The effects of cyanotoxins on terrestrial animals (e.g., dogs, cattle, and birds) and humans range from contact irritation to gastrointestinal distress to acute, chronic and lethal poisoning (Breinlinger et al., 2021). cHABs are predicted to become more frequent and severe with climate change (Huisman et al., 2018; Ho et al., 2019). Hence, it is imperative to understand the effects of cyanotoxins, including their risk to human health (Jones et al., 2021). *Microcystis aeruginosa*, the dominant species in cHABs, releases exudates that cause a variety of impairments in other algae (Wang et al., 2017; Pei et al., 2019), higher plants (Xu et al., 2015; Xu et al., 2016), waterfleas (Xu et al., 2019), and fish (Zi et al., 2017). We investigated the metabolic profiles of *M. aeruginosa* exudates in exponential and stable growth phases to identify their active compounds. Phytosphingosine (PHS) was identified as the key exudate (Zhou et al., under review; Jiayao, 2021) and was produced at a concentration of 0.9–2.9 μg/L (Figs. S1; S2). However, its association with adverse outcomes in aquatic biota remains unclear. PHS is a unique component of sphingolipids in that it possesses a hydroxyl group at C-4 of the sphingoid long-chain base. This chemical is present in yeast, plant, and animals, including humans (Kondo et al., 2014). Li et al. (2020) isolated PHS from wheat root exudates and identified it to be an antifungal compound. Moreover, PHS and its derivatives have been used in cosmetics for skin protection, such as preventing wrinkles (Choi et al., 2017). The PHS-related sphingolipid metabolites ceramide, sphingosine, and sphingosine-1-phosphate have been shown to induce programmed cell death (Taha et al., 2006). Multiple mechanisms mediate

* Corresponding authors.
E-mail addresses: xchang@uwindsor.ca (X. Chang), cuiqinghua@ynu.edu.cn (Q. Cui).
[1] Jiaojiao Li and Jiayao Wen contributed equally to this work.

https://doi.org/10.1016/j.tox.2022.153370
Received 27 July 2022; Received in revised form 27 October 2022; Accepted 31 October 2022
Available online 9 November 2022

sphingosine-driven cell death. Studies with different types of cells and models support the role of sphingolipids, mainly ceramides and sphingosine-1-phosphate, as regulators of mitochondrial dynamics via fission, fusion, and mitophagy (Fugio et al., 2020). PHS has been classified as a corrosive and environmentally hazardous substance by the European Chemicals Agency. It is highly toxic to aquatic life and exerts long-lasting effects (EPA, 2021). Because PHS showed strong cytotoxicity on Chinese hamster ovary cells and mitochondria (Lee et al., 2001), we hypothesized that it could act as one of the drivers of mitochondrially mediated cytotoxicity.

Mitochondria are responsible for most of the metabolic activities in cells, including regulation of cellular metabolism, ROS (reactive oxygen species) generation, and calcium homeostasis (Murphy and Steenbergen, 2020). Additionally, mitochondria are the primary structures that control cell death, including apoptosis, and extrinsic and intrinsic cascades (Jodeiri Farshbaf and Ghaedi, 2017). PHS induces cytotoxicity; for example, it has been reported to induce the apoptosis of Jurkat and NCI-H460 cells via the caspase-8 and mitochondria-mediated pathways, downregulation of ERK activity, and activation of P38 MAPK (Park et al., 2003). Furthermore, PHS can directly or indirectly interfere with mitochondria and induce their apoptosis (Nagahara et al., 2005), but the underlying mechanism is yet to be elucidated. Mitophagy is a mitochondrial self-repair system that removes damaged mitochondria and maintains the quantity and quality of healthy mitochondrial mass (Schofield and Schafer, 2021). Mitophagy is important because its disruption promote apoptosis.

In vitro methods, including cell tests, are important for developing a systematic and predictive assessment of possible environmental risks from chemicals and complex mixtures (Rehberger et al., 2018). In this study, we selected CNE-2 cells to illustrate the cytotoxicity mechanism of PHS-induced cytotoxicity by comparing the sensitivities of several cell lines, namely, the human promyelocytic acute leukemia cell line HL-60, the human hepatocellular carcinoma cell line HepG2, the human kidney epithelial cell line 293 T, and the human non-small-cell lung cancer cell line H1299 (Fig. S3). The objectives of our study were to: 1) evaluate the cytotoxicity of PHS; 2) investigate changes in mitochondrial structure after exposure to PHS and determine the functions of PHS; and 3) identify the underlying mechanism of PHS-induced cytotoxicity.

2. Materials and methods

2.1. Reagents

PHS (CAS:554–62–1) was purchased from Shanghai Yuanye Bio-Technology (Shanghai, China). Fluorescent probes (Annexin V-FITC, DCFH-DA, Mitosox Red, Calcein-AM, and JC-1), ATP detection kit, Cell Counting Kit-8, and Cell Mitochondria Isolation Kit were purchased from Beyotime Biotechnology (Shanghai, China). Dimethyl sulfoxide (DMSO) was purchased from Solarbio Life Science (Beijing, China). Cytochrome-c, Parkin, P62, Bax, and Bcl2 antibodies were purchased from Cell Signaling Technology (Danvers, MA, USA). PINK1 antibody was purchased from Proteintech (Wuhan, China). Glyceraldehyde-3-phosphate dehydrogenase (GAPDH) antibody, Cytochrome c oxidase IV (COX IV) antibody, Alexa Fluor 488-labeled Goat Antirabbit IgG (H + L), and Alexa Fluor 488-labeled Goat Anti-Mouse IgG (H + L) were purchased from Beyotime Biotechnology (Shanghai, China).

2.2. Cell culture

Human cells used in this study were reviewed and approved by an accredited committee at Yunnan University. CNE-2 cells were maintained in Dulbecco's Modified Eagle's Medium (DMEM; Gibco, Thermo Fisher Scienfific, Waltham, MA, USA) supplemented with 10% fetal bovine serum and 1% penicillin-streptomycin. The Cell Counting Kit-8 (CCK-8) assay kit (Beyotime) was used to measure the viability of CNE-2 cells. Approximately, 5×10^3 CNE-2 cells (cells/per well) were seeded into a 96-well plate and cultured at 37 ℃ and 5% CO_2. After 24 h, the cells were separately treated with 0, 10, 20, or 30 μM of PHS for 48 h. Subsequently, 20 μL of CCK-8 solution and 80 μL of fresh DMEM were added to each well, and the cells were cultured under the same conditions as earlier. The absorbance of the cell culture was measured at 450 nm using a microplate spectrophotometer. Thereafter, the half-maximal inhibitory concentration (IC_{50}) against PHS and the associated 95% confidence interval were evaluated.

2.3. Flow cytometry to measure cell apoptosis

An Annexin V-FITC apoptosis detection kit was used to measure cell apoptosis. Cells were obtained from a six-well plate after treatment with 10, 20, or 30 μM of PHS. Cells were then transferred to a 15 mL centrifuge tube and resuspended in 195 μL of 1 × binding buffer. Annexin V-FITC (5 μL) and propidium iodide (PI, 10 μL) were added, and the tubes were incubated for 20 min in the dark at room temperature after vortexing gently. Finally, flow cytometry was used to analyze cell apoptosis in the samples. FlowJo software was used for subsequent data processing.

2.4. Determination of mitochondrial membrane potential

Cells were treated with 10, 20, or 30 μM of PHS for 48 h in a six-well plate. Fresh DMEM mixed with JC-1 working solution was then added and the cells were incubated for 20 min in at 37 ℃. The cells were then washed three times with JC-1 buffer (1 ×) to replace the fresh DMEM. Finally, a fluorescence microscope (Olympus, Tokyo, Japan) was used to measure the changes of mitochondrial membrane potential. The ratio of the fluorescence value of the exposed group to that of the control group was used to estimate the relative mitochondrial membrane potential.

2.5. Measurement of ATP generation

After exposure to 10, 20, or 30 μM of PHS for 48 h, the cells were lysed with 200 μL/well of ATP lysates. The supernatant was collected via centrifugation at 12,000g for 5 min at 4 ℃. Subsequently, 100 μL of ATP test-working solution was added to each test tube, after which the solution was left to stand for 5 min at room temperature. Thereafter, 20 μL of the sample was introduced into the ATP assay tube and mixed rapidly with a micropipette. The relative light unit value was measured with a luminometer set for chemiluminescence detection.

2.6. Transmission electron microscopy

Cells treated with 10, 20, or 30 μM of PHS were mixed with 2.5% glutaraldehyde overnight. They were then fixed in 2% osmium tetroxide after 1 h of staining with 2% uranyl acetate. Samples were scratched and embedded in Durcopan ACM for 6 h, and stained with uranyl acetate and lead citrate. A Zeiss EM900 transmission electron microscope (TEM, Gottingen, Germany) was used to analyze the microstructure of the cells.

2.7. Isolation of cytoplasm and mitochondria

The cells were inoculated into 60 mm plates, followed by treatment with 10, 20, or 30 μM of PHS for 48 h. Approximately 4×10^7 cells were collected by centrifugation at 600g and 4 ℃ for 5 min and then suspended in 500 μL of separation buffer. The cells were homogenized 30 times on ice with a glass homogenizer, and then centrifuged at 600 g for 10 min at 4 ℃ to obtain the supernatant. It was centrifuged at 11, 000g for 10 min at 4 ℃ to collect the mitochondria in the precipitate. And the remaining liquid was collected as the cytoplasm, centrifuged at 12,000 g for 10 min at 4 ℃, the supernatant was applied to run the western blotting. Mitochondria were lysed and detected by the western blotting. Both were probed with mitochondrial marker COX IV and cytosolic GAPDH.

2.8. Determination of intracellular / mitochondrial ROS generation

The cells were inoculated into six-well plates, and DCFH-DA/Mitosox Red fluorescent dye was added at a final concentration of 5 μM after treatment with 10, 20, or 30 μM of PHS for 48 h. Subsequently, the cells were incubated for 30 min at 37 ℃. They were than rinsed with serum-free cell inoculation medium three times to remove DCFH-DA/Mitosox Red fluorescent dye. The levels of intracellular/mitochondrial ROS production were determined using a fluorescence microscope or multi-functional fluorescence microplate reader.

2.9. Measurement of mitochondrial Ca^{2+} level

Rhod2-AM was dissolved in DMSO to form a 5-mM stock solution. An aliquot of this stock solution was diluted in 4 μM of phosphate buffered saline (PBS) to obtain the working solution. The cells were inoculated into a 96-well black-bottomed plate, followed by treatment with 10, 20, or 30 μM of PHS for 48 h. After being loaded with Rhod2-AM working solution for 30 min at 37 ℃, the cells were washed twice with PBS. Finally, the relative Ca^{2+} level in the mitochondria was measured using a microplate spectrophotometer.

2.10. Determination of the degree of openness of mitochondrial permeability transition pores

The CNE-2 cells were inoculated into a black-bottomed 96-well plate, followed by treatment with 10, 20, or 30 μM of PHS for 48 h. After adding 100 μL of calcein-AM staining solution, 100 μL of fluorescence quenching working solution, and 100 μL of ionomycin control, the plates were shaken gently so that the dye evenly covered all the cells. Later, the cells were incubated in the dark at 37 °C for 30 min. The solution was then replaced with fresh preheated DMEM, and the plates were incubated at 37 °C for 30 min in the dark to produce green fluorescent calcein. Subsequently, the culture medium was aspirated, washed 2–3 times with PBS, and detection buffer was added before the cells were measured with a microplate spectrophotometer.

2.11. Western blotting

The cells were inoculated into 60-mm plates and exposed to 10, 20, or 30 μM of PHS for 48 h. After 48 h, the cells were rinsed with ice-chilled PBS and lysed with radioimmunoprecipitation assay (RIPA) lysis buffer. To extract the total protein from the CNE- 2 cells, samples were homogenized with 1% PMSF in RIPA lysis buffer (Beyotime) for 30 min on ice and centrifuged at 12,000g for 15 min at 4 °C. Protein concentration was then determined using a bicinchoninic acid kit (BCA; Dingguo Changsheng Biotechnology, Beijing, China). Protein samples were loaded into the electrophoresis system with 12.5% separation gel and 5% concentration gel and then electrotransferred to a polyvinylidene fluoride membrane. Next, 5% nonfat dry milk was used to block the membranes for approximately 2 h at room temperature. After 2 h, the membranes were washed with phosphate-buffered saline with Tween 20 (PBST) three times (5 min each). Next, the membranes were incubated with primary antibodies overnight at 4 ℃. Blots were developed by incubation with the corresponding secondary-antibody for 2 h at room temperature after washing with PBST buffer. After rinsing and washing three times with PBST, the immune complexes were visualized using the Gel Imaging System (Tanon, Shanghai, China).

2.12. Statistical analysis

All values were expressed as mean ± SD of three independent experiments. One-way analysis of variance (ANOVA) was used, followed by Duncan's multiple comparison test with SPSS (version 25: IBM) to identify significant differences between the control and treatment groups.

3. Results

3.1. PHS induced cytotoxicity in CNE-2 cells

Upon treatment with 10 or 20 μM of PHS for 48 h, cell viability declined from 91.3% to 71.3%, and the decrease was even more pronounced upon treatment with 30 μM treatment (91.3–52.6%; $P \leq 0.05$) (Fig. 1). PHS induced cytotoxicity in a dose- and time-dependent manner. We selected concentrations of 10, 20, and 30 μM for subsequent experiments.

3.2. Ultrastructural analysis revealed that PHS inflicted mitochondrial damage

TEM analysis revealed clear ultrastructural changes in mitochondria in the cells treated with all three tested PHS concentrations (10, 20, and 30 μM) after 48 h of exposure (Fig. 2). The number of swollen mitochondria increased markedly, as did the occurrence of disordered cristae and the rupture of the mitochondrial membrane. The treatments with 10 μM and 20 μM of PHS did not lead to obvious expansion of the rough endoplasmic reticulum (RER), and attached ribosomes were visible on the surface (Fig. 2b1 and c2). However, in the 30-μM group, the RER was expanded, and degranulation was apparent (Fig. 2a4 and b4). Damaged mitochondria, with the features of swelling, rupture of the mitochondrial membrane, and fracture of the mitochondrial cristae, were counted (Fig. 4c). The number of damaged mitochondria in the cells was significantly increased ($P \leq 0.05$) in the treated groups, especially in the group treated with 30 μM of PHS.

3.3. PHS exposure increased both intracellular and mitochondrial ROS levels, increased mitochondrial membrane potential (MMP) disruption, and decreased ATP content in CNE-2 cells

When exposed to PHS at concentrations of 10, 20, or 30 μM, relative intracellular ROS levels increased to 1.3, 1.47, and 1.2 times those of the control group, respectively ($P < 0.01$; Fig. 3B and C). Intracellular ROS of CNE-2 were measured with DCFH-DA green fluorescence staining assay, and the fluorescence intensity was found to be significantly increased by the treatments (Fig. 3E). The generation of intracellular ROS increased in a manner dependent on the dose of PHS.

The fracture of mitochondrial cristae was observed using TEM after treatment with PHS. ATP content decreased significantly after PHS treatment for 48 h in a concentration-dependent manner ($P < 0.01$). For

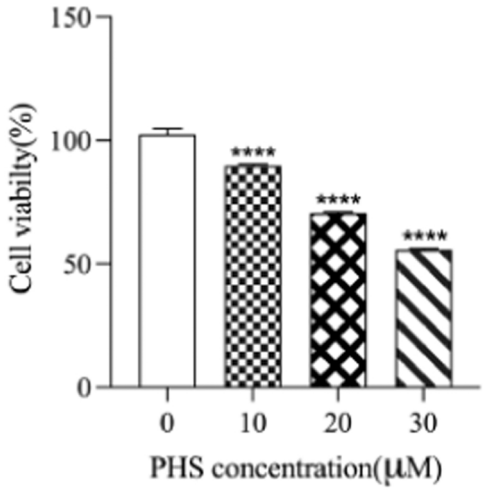

Fig. 1. Mean (± SD) reduction of cell viability of CNE-2 cells upon exposure to phytosphingosine (PHS) for 48 h. n = 3. Bars marked with an asterisk are significantly different from the control ($P \leq 0.05$).

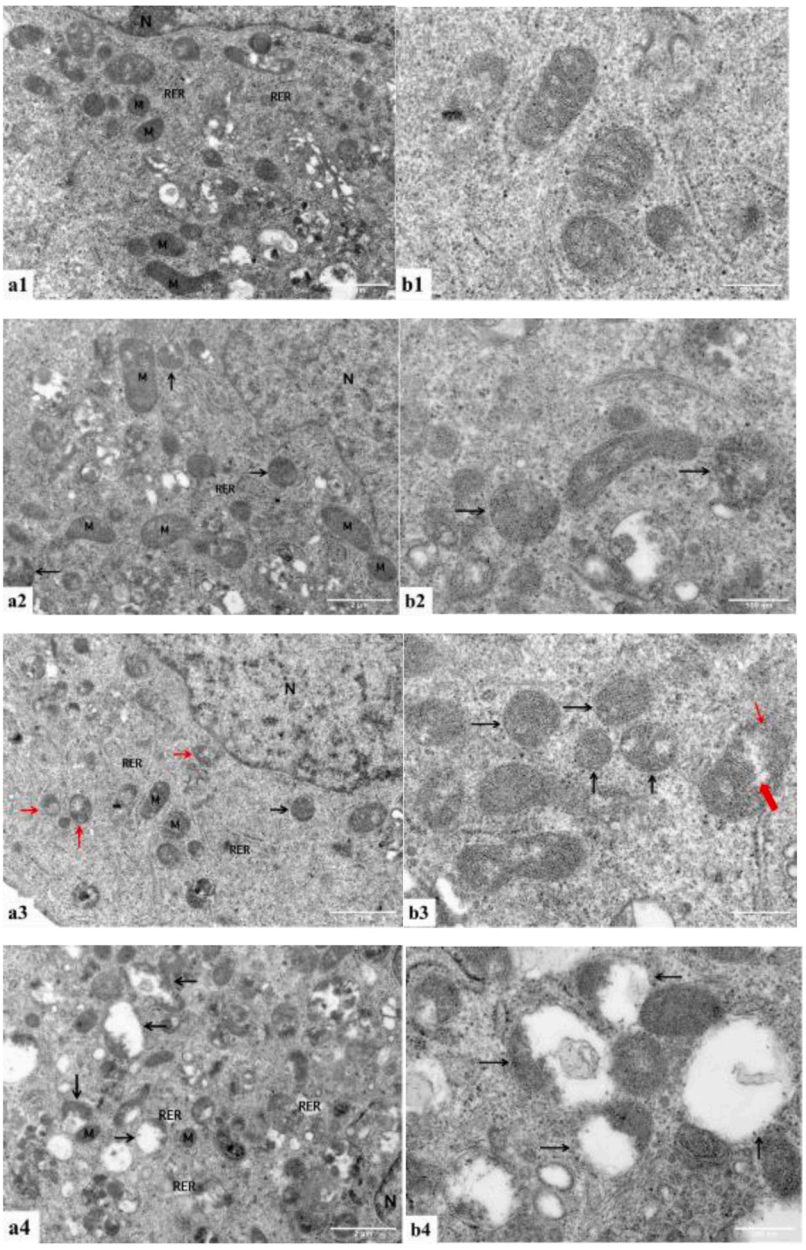

c

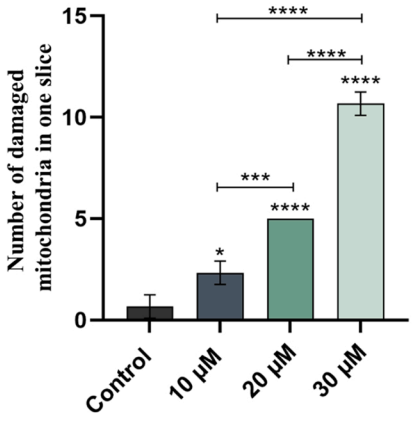

Fig. 2. TEM images for ultrastructural observation of CNE-2 cells after treatment with different concentrations (10, 20, and 30 μM) of PHS for 48 h. Control group (a1, b1); 10 μM PHS-treatment (a2, b2); 20 μM PHS-treatment (a3, b3); 30 μM PHS-treatment (a4, b4); the average number of damaged mitochondria from a TEM slice of 2-μm scale bar (c). N, nucleus; M, mitochondrion; RER, rough endoplasmic reticulum. Thick red arrow (in b3) indicates fracture of mitochondrial cristae. Thin red arrow (in a3, b3) indicates rupture of mitochondrial membrane. Black arrows (in a2, a3, b2, b3, b4) indicate swollen mitochondria. Scale bar: 2 μm in a1-a4, 500 nm in b1–b4.

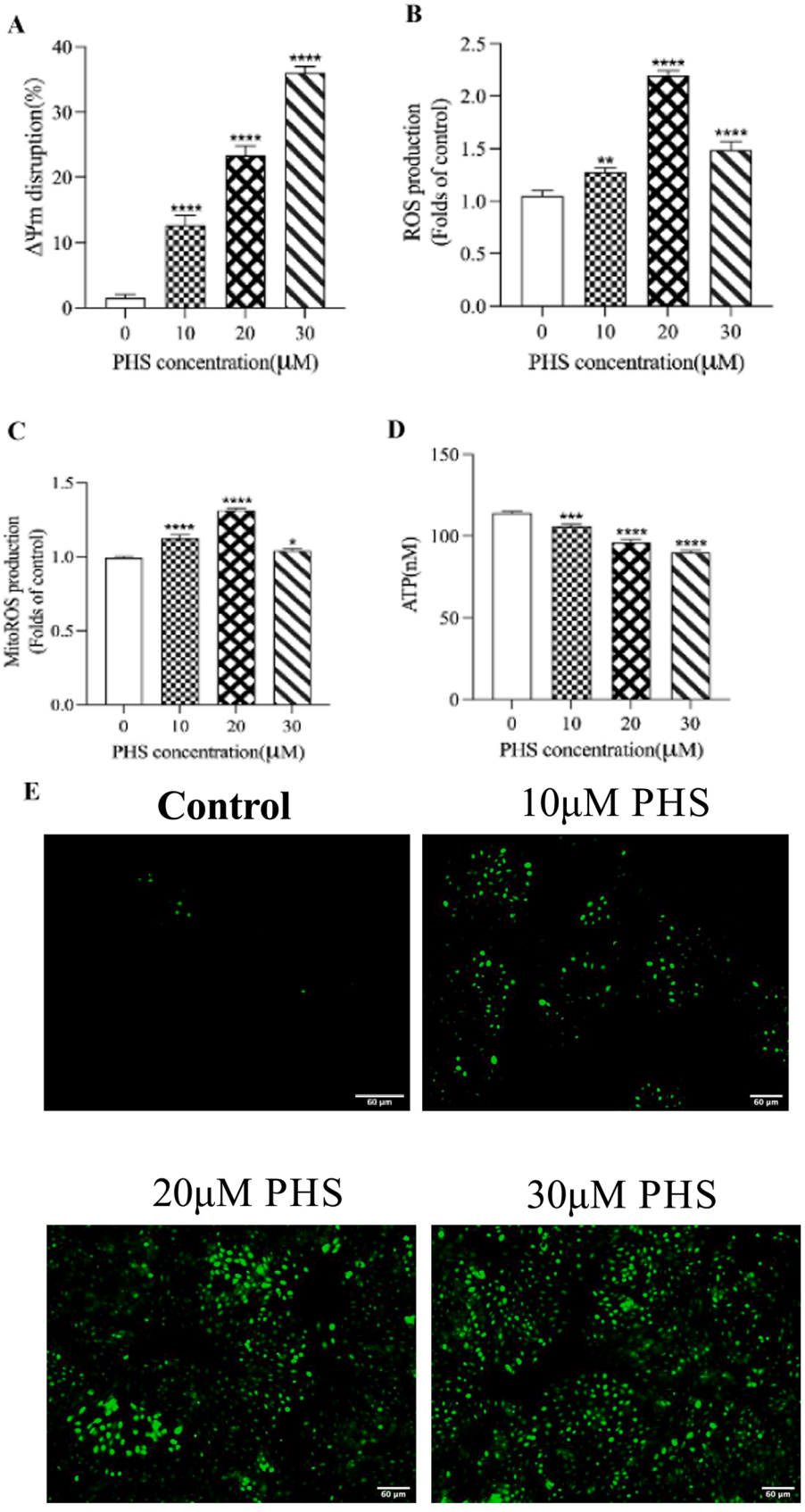

Fig. 3. Disintegration of mitochondrial membrane potential (A), intracellular and mitochondrial ROS levels (B and C), ATP production levels (D), and DCFH-DA staining were analyzed to examine intracellular ROS with green fluorescence at excitation/emission wavelengths of 488/525 nm. (E) in CNE-2 cells after PHS (0, 10, 20, or 30 μM) exposure for 48 h. All values are mean ± SD; n = 3. Bars significantly different from the control are indicated by * ($P < 0.05$), * * ($P < 0.01$), * ** ($P < 0.005$) or * *** * ($P < 0.001$).

example, ATP content decreased from 112 to 87 nM after exposure to 30 μM of PHS for 48 h (Fig. 3D). Decoupling of oxidative phosphorylation disrupts electron gradients across membranes, which leads to decrease in the mitochondrial membrane potential (MMP), as a marker of mitochondrial health. The relative permeabilization ratio of MMP in CNE-2 cells was elevated 6.0–15.6 times that relative to that in the control group following exposure to 10–30 μM of PHS (Fig. 3A). Thus, PHS appears to cause mitochondrial dysfunction in CNE-2 cells.

3.4. Mitochondrial Ca^{2+} overload by PHS induced partial opening of mitochondrial permeability transition pores, which further induced mitochondrially mediated apoptosis in CNE-2 cells

Mitochondrial Ca^{2+} was overloaded after 48 h in PHS treatments relative to that in the control group (Fig. 4A). The relative expression of mitochondrial calcium uniporter (MCU), which is essential for mitochondrial Ca^{2+} uptake, was upregulated in a concentration-dependent manner upon PHS treatment ($P < 0.05$; Fig. 4A and B).

The degree of opening of mitochondrial permeability transition pores (mPTPs) increased to 117% in the 30-μM PHS group ($P < 0.01$; Fig. 4D). Based on these results, PHS seems to induce apoptosis in CNE-2 cells.

We verified early- and late-apoptotic cells after treatment with 10—30 μM of PHS using Annexin V and PI staining (Fig. 4E). PHS elevated the late-apoptotic cell population of CNE-2 cells by 77% compared with that of the vehicle-treated cells. Mitochondrially related proteins (cytochrome c Mito) were analyzed using the mitochondrial protein COX IV as a control, and cytosolic proteins (cytochrome c Cyto) were analyzed using GAPDH (Glyceraldehyde-3-phosphate dehydrogenase) as a housekeeping gene. The expression of the apoptosis-related proteins Bax, Bcl-2, cytochrome-c, and cleaved caspase-3 reflected the degree of apoptosis. For example, the expression of Bax increased and that of Bcl-2 decreased when compared with the levels in the control group (Fig. 5A). The relative protein expression of cytochrome-c decreased in the mitochondria and increased in the cytoplasm after exposure to PHS (Fig. 5B and D), which indicated a directional release. Furthermore, the expression of cleaved caspase-3 protein upon treatment with 30 μM of PHS increased 1.73-fold compared with that in the control ($P < 0.01$; Fig. 5B), which corresponded with the rate of cell apoptosis detected via staining. Thus, PHS induces mitochondrial dysfunction and further activates mitochondrially mediated apoptosis in CNE-2 cells.

3.5. PHS decreased PINK1/Parkin-mediated mitophagy in CNE-2 cells

PINK1 protein expression was significantly downregulated compared with that in the control group ($P < 0.01$; Fig. 6B). The expression of P62 was also downregulated (Fig. 6D), as was that of Parkin in the mitochondria and cytoplasm ($P < 0.01$) (Fig. 6C). These results reveal that PHS blocks the PINK1/Parkin mitophagy pathway in CNE-2 cells.

4. Discussion

Cyanobacteria produce many secondary metabolites with strong biological activities, including acute toxicity to animals and humans (Liyanage et al., 2016). In this study, we found that acute exposure to PHS caused cytotoxicity in human CNE-2 cells. We propose that the mechanism of cytotoxicity is damage to mitochondrial structure and function, accompanied by PINK1/Parkin-mediated blockage of mitophagy. These processes eventually lead to cell death via the mitochondrially mediated apoptotic pathway.

Mitochondria are responsible for most metabolic activities in cells (Genovese et al., 2021). However, antioxidant system overloading, oxidative stress and mitochondrial damage could result from the excessive production of ROS (Yang and Lian, 2020). Our results showed that PHS significantly enhanced ROS levels in CNE-2 cells, which damaged the mitochondrial structure. Structural damage to mitochondria has been reported to lead to mitochondrial dysfunction and cause further damage to cells and tissues, eventually resulting in cell death (Ostaszewska-Bugajska et al., 2022).

Oxidative stress from excessive cellular production of ROS causes damage to DNA and MMP and induces apoptosis (Singh et al., 2019). A decrease in MMP is generally considered to be a late event in the apoptotic pathway (Ly et al., 2003). During energy production, nutrient metabolism forms a proton gradient in the inner mitochondrial membrane, which drives ATP production; on the contrary, a reduction in MMP blocks the supply of mitochondrial energy (de la Fuente-Herreruela et al., 2017). As we expected, excessive cellular ROS production disrupted mitochondrial membrane permeability, and the disintegration of MMP increased in a concentration-dependent manner. This process is similar to BEAS-2B cell apoptosis, as reported by Cao et al. (2021).

Fracture of mitochondrial cristae interrupts ATP synthesis, which induces mitochondrial dysfunction. We found that ATP content was significantly reduced after PHS treatment for 48 h in a concentration-dependent manner ($P < 0.01$), which combined with ROS accumulation, led to mitochondrial dysfunction. We observed that intracellular and mitochondrial ROS levels were reduced upon treatment with 30 μM of PHS compared with those with 20 μM of PHS, although ROS production at the former concentration was still higher than that in the control without PHS exposure (Fig. 3B and C). We predicted this result because ROS were produced by mitochondria in cells whose viability was decreased to 52.6% upon treatment with 30 μM of PHS (Fig. 1). In addition, at this PHS concentration, we noted that the structure of mitochondria was disrupted, with the appearance of degranulation (Figs. 2a4 and b4). We anticipated that more than half of the cells would be damaged or dead, perhaps triggered by their repair feedback loop to reduce ROS production.

The disintegration of MMP is a prerequisite for the dysregulation of calcium homeostasis. The MCU protein, which transports Ca^{2+} into the mitochondria, plays an important role in maintaining Ca^{2+} homeostasis in the physiological state (Paillard et al., 2018). Under stress, overactivation of MCU can lead to mitochondrial Ca^{2+} overload, oxidative phosphorylation, ROS overproduction, decrease in MMP, and release of proapoptotic factors, thereby resulting in apoptosis (Wang et al., 2015). Here, we observed that the expression of MCU was upregulated after PHS exposure, thus inducing further mitochondrial Ca^{2+} overload. Disruption of Ca^{2+} and ROS homeostasis can lead to mitochondrial damage and dysfunction (Park et al., 2022). Mitochondrial Ca^{2+} overload due to MCU activation, in turn, leads to mPTP opening and the release of apoptotic factors (Danese et al., 2017). Our results are consistent with this model as PHS-exposed cells experienced elevated opening of mPTPs, with Ca^{2+} overload and excessive production of ROS. These findings are consistent with the disruption of the mitochondrial membrane structure, as revealed by ultrastructural observation.

Based on the mitochondrial dysfunction in CNE-2 cells, we speculate that the activation of mitochondrially mediated apoptotic signals might have occurred. During apoptosis, mitochondrial dysfunction is commonly triggered by different cellular stresses, aberrant expression of Bax, and Bcl-2, and cascade activation of downstream caspase families, including caspase-3, 6, 7, and 9, which are associated with apoptosis (Abate et al., 2020). Moreover, the ratio of proapoptotic members to the level of Bax in the mitochondria has been reported to be closely related to cell survival and apoptosis (Song et al., 2011). In our study, the mitochondrially mediated intrinsic apoptotic pathway was activated after PHS exposure. We detected early- and late-apoptotic cells with flow cytometry. Our results indicated that the expression of Bax/Bcl2 was upregulated after PHS exposure and that cytochrome c was released from the mitochondria into the cytoplasm. This release activated caspase-3 further downstream, thereby inducing apoptosis in CNE-2 cells. The same mitochondrially mediated apoptotic mechanism has

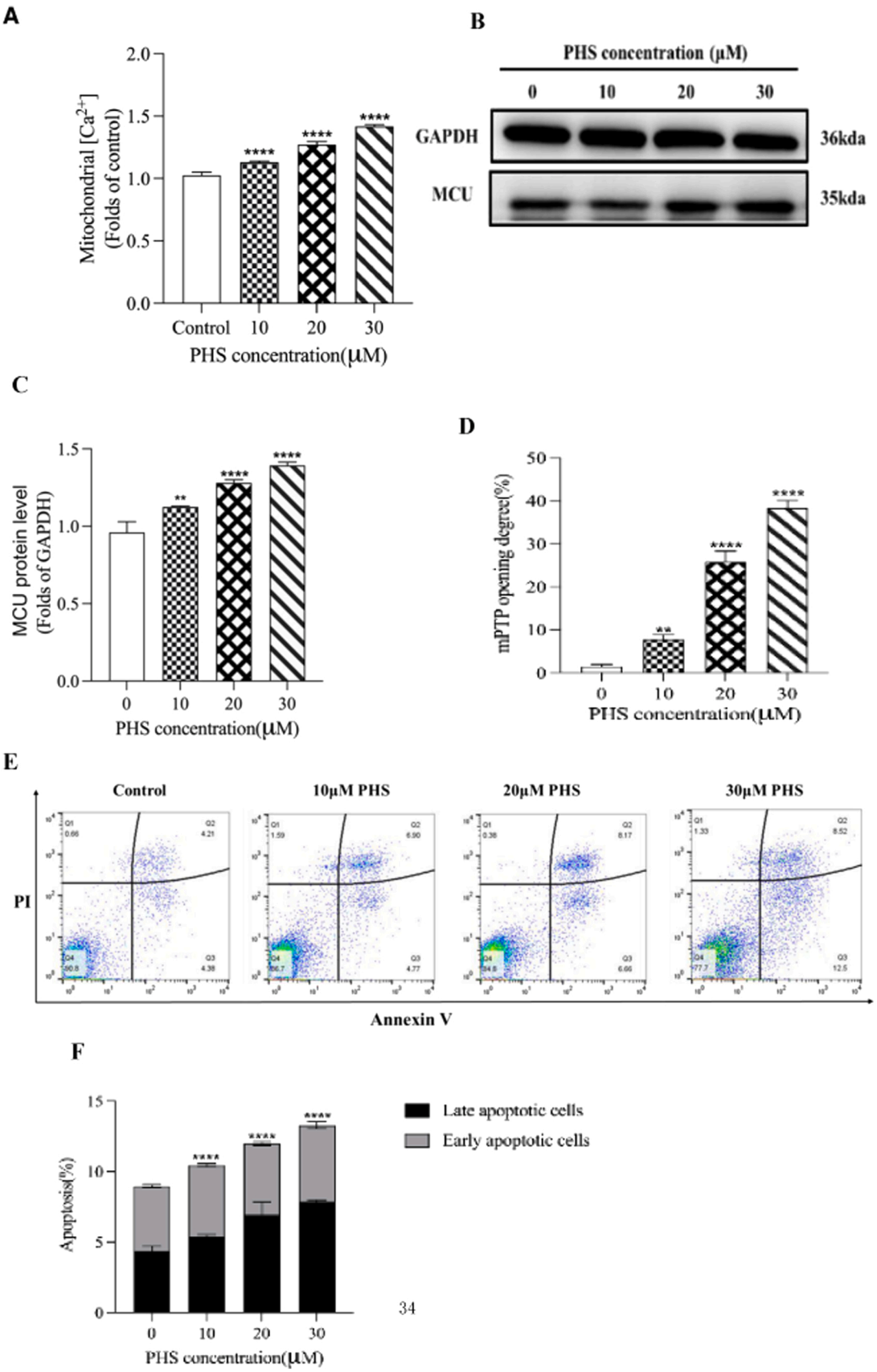

Fig. 4. After exposure of PHS (0, 10, 20, or 30 μM) for 48 h, CNE-2 cells were given different treatments to evaluate mitochondrial Ca^{2+} level (A), MCU protein expression (B), MCU protein expression level (C), mPTP opening degree (D), cell apoptosis (E), proportion of early- and late-apoptotic cells (F). MCU, mitochondrial calcium uniporter. *Significantly different from control ($P \leq 0.05$) (one-way ANOVA followed by Duncan's multiple comparison test).

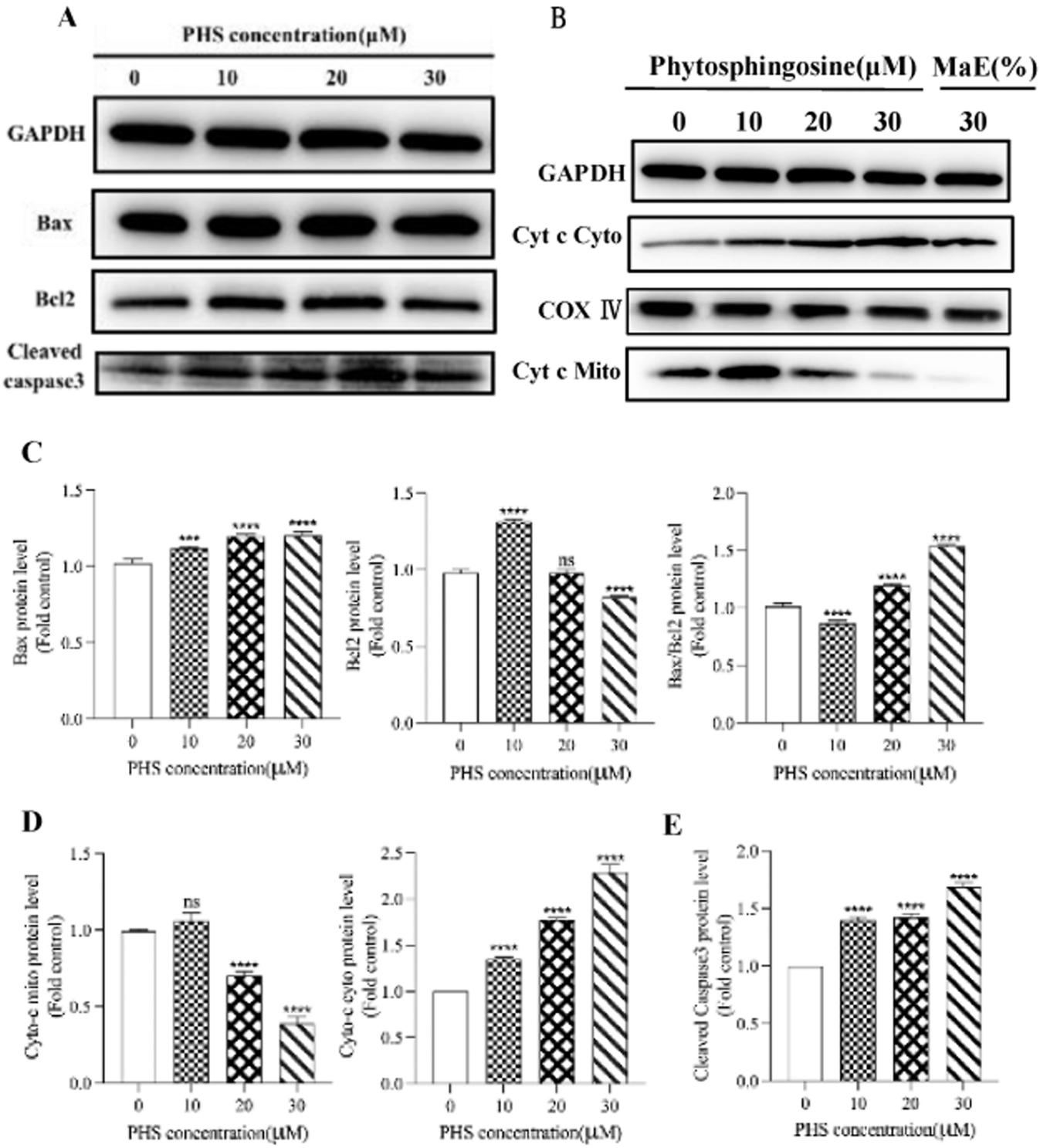

Fig. 5. PHS induced the mitochondrially mediated apoptosis pathway in CNE-2 cells. (A) CNE-2 cells were exposed to PHS (0, 10, 20, or 30 μM) for 48 h. Bax, Bcl2, and Bax/Bcl2 expressions were analyzed with western blotting. (B) Cytochrome-c protein expression in both mitochondrial and cytosolic fractions was analyzed with western blotting. (C) Bax, Bcl2, and Bax/Bcl2 protein expression levels were quantified. (D) Cytochrome-c protein expression levels in both the mitochondria and the cytosol were quantified. (E) Cleaved caspase-3 protein expression level was quantified. *Significantly different from control ($P \leq 0.05$) (One-way ANOVA followed by Duncan's multiple comparison test).

been observed after PHS exposure in Jurkat cells (Park et al., 2003). These results suggest that PHS can induce apoptosis via the caspase-dependent pathway in CNE-2 cells and that the occurrence of apoptosis is related to mitochondrial damage.

Mitophagy acts as a pro-survival system for cells under acute and chronic stimuli by maintaining mitochondrial homeostasis (Lou et al., 2020). Oxidative stress and hypoxic conditions are critical factors that contribute to mitophagy. Both can result in the deterioration of mitochondrial functions and structure (Kulikov et al., 2017). Our results demonstrate that the expression of Parkin protein was reduced in the mitochondria and cytoplasm and that PINK1 expression was also downregulated. This finding suggests that PINK1 failed to recruit Parkin

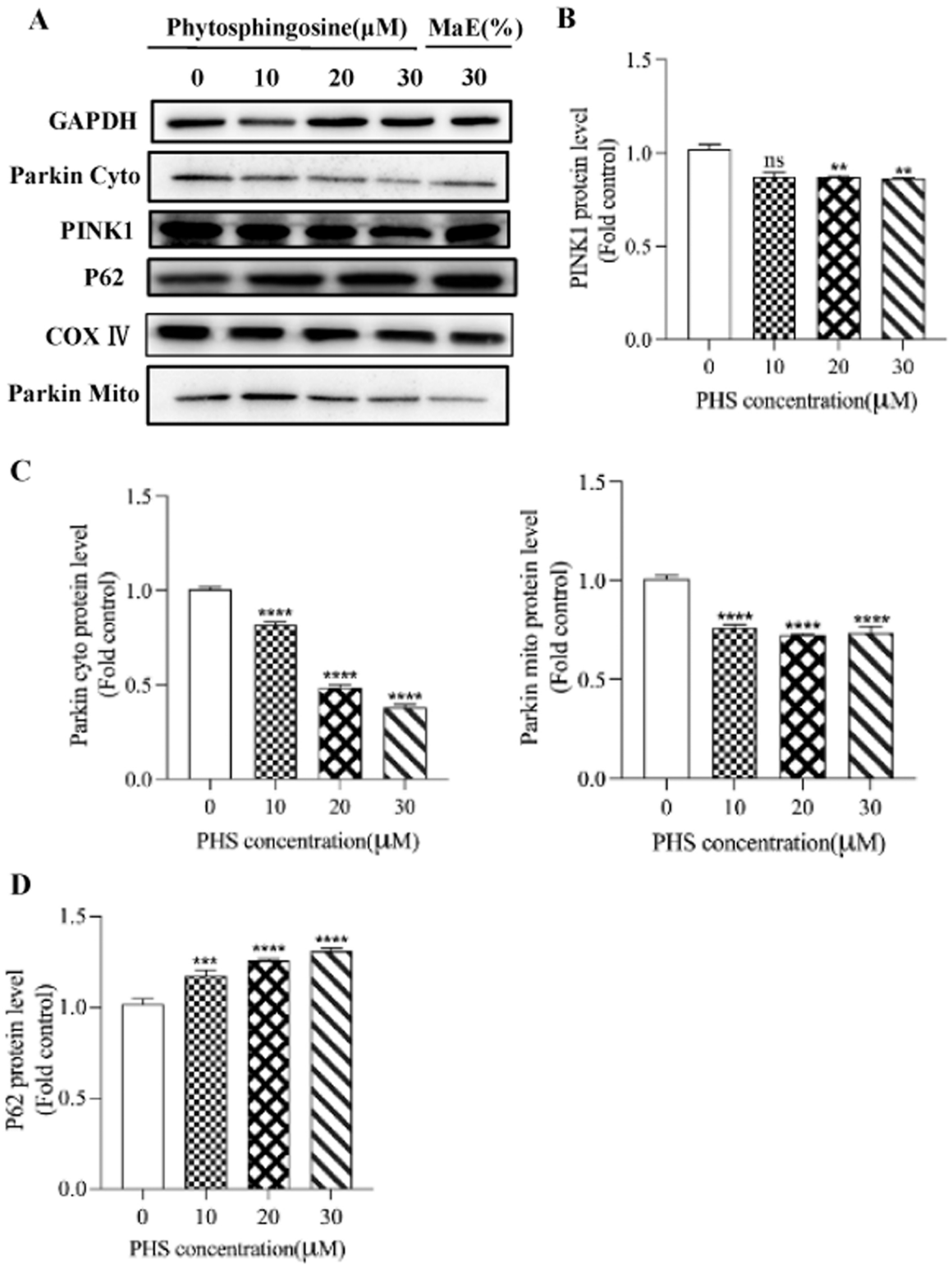

Fig. 6. PHS blocked PINK1/Parkin-mediated mitophagy in CNE-2 cells. (A) After exposure to PHS (0, 10, 20, or 30 μM) for 48 h, the expression level of Parkin, PINK1, and P62 were analyzed using western blotting. (B) PINK1 protein expression level. (C) Parkin protein expression levels in both mitochondrial and cytosolic fractions. (D) P62 protein expression level. *Significantly different from control ($P \leq 0.05$) (one-way ANOVA followed by Duncan's multiple comparison test).

to the mitochondria, thus blocking PINK1/Parkin-mediated mitophagy. In summary, we speculate that there is a causal relationship exists between apoptosis and mitophagy, i.e., the inhibition of PINK1/Parkin-mediated mitophagy promoted apoptosis. Furthermore, the overexpression of Parkin may reduce the number of dysfunctional mitochondria and lower the occurrence of apoptosis, thereby increasing cell viability. However, these hypotheses need to be confirmed in future studies.

PHS is found in the small intestine and skin of animals, including humans (Breimer et al., 1975). PHS has several useful functions including its use in cosmetics (Fischer et al., 2012) or as an antibacterial and anti-inflammatory agent to prevent or treat abnormal skin

conditions (e.g. acne) (Pavicic et al., 2007). However, its use in these applications requires careful consideration of the dose, given its cytotoxicity and biological toxicity. We propose that PHS concentration be closely monitored in cHAB, along with those of other compounds of concern that are released by cyanobacterial cells (microcystin-LR and anatoxin-a).

5. Conclusion

Our study found that the exposure of human CNE-2 cells to PHS causes excessive production of ROS and results in structural damage to the mitochondria. Specifically, PHS exposure causes mitochondrial membrane rupture, thereby leading to MMP disintegration and mitochondrial Ca^{2+} overload. The expression of Bax and Bcl2 proteins are significantly upregulated upon exposure to PHS. The opening of mPPTs opening with pores formed by Bax dimers promotes the release of cytochrome c into the cytoplasm. Mitochondrially mediated apoptotic pathway is induced when cytochrome c activates downstream caspase-3. PHS exposure also decreases the expression of the mitophagy-associated proteins PINK1 and Parkin and upregulates the expression of P62 protein. These changes lead to a failure of Parkin into the mitochondria to activate mitophagy, thereby promoting apoptosis and cell toxicity. Thus, cyanobacteria-derived PHS requires monitoring during freshwater cHAB blooms to ensure the supply of safe drinking water.

Declaration of Competing Interest

The authors declare that they have no known competing financial interests or personal relationships that could have appeared to influence the work reported in this paper.

Data Availability

Data will be made available on request.

Acknowledgements

This research was financially supported by the National Natural Science Foundation of China (Nos: U1902202; 32101361; 32060161); Great Lakes Fishery Commission (2020_MAC_440940); Yunnan Provincial Science and Technology Department grants (2019FA043; 2019BC002; 202101AU070078; 202201AT070177), and an NSERC Discovery grant. We also thank Servicebio company for assistance with TEM analysis.

Appendix A. Supporting information

Supplementary data associated with this article can be found in the online version at doi:10.1016/j.tox.2022.153370.

References

Abate, M., Festa, A., Falco, M., Lombardi, A., Luce, A., Grimaldi, A., Zappavigna, S., Sperlongano, P., Irace, C., Caraglia, M., Misso, G., 2020. Mitochondria as playmakers of apoptosis, autophagy and senescence. Semin Cell Dev. Biol. 98, 139–153. https://doi.org/10.1016/j.semcdb.2019.05.022.

Breimer, M.E., Karlsson, K.A., Samuelsson, B.E., 1975. Presence of phytosphingosine combined with 2-hydroxy fatty acids in sphingomyelins of bovine kidney and intestinal mucosa. Lipids 10 (1), 17–19. https://doi.org/10.1007/bf02532188.

Breinlinger, S., Phillips, T.J., Haram, B.N., Mareš, J., Martínez Yerena, J.A., Hrouzek, P., Sobotka, R., Henderson, W.M., Schmieder, P., Williams, S.M., Lauderdale, J.D., Wilde, H.D., Gerrin, W., Kust, A., Washington, J.W., Wagner, C., Geier, B., Liebeke, M., Enke, H., Niedermeyer, T.H.J., Wilde, S.B., 2021. Hunting the eagle killer: a cyanobacterial neurotoxin causes vacuolar myelinopathy. Science 371 (6536), eaax9050. https://doi.org/10.1126/science.aax9050.

Cao, X., Fu, M., Bi, R., Zheng, X., Fu, B., Tian, S., Liu, C., Li, Q., Liu, J., 2021. Cadmium induced BEAS-2B cells apoptosis and mitochondria damage via MAPK signaling pathway. Chemosphere 263, 128346. https://doi.org/10.1016/j.chemosphere.2020.128346.

Choi, H.K., Cho, Y.H., Lee, E.O., Kim, J.W., Park, C.S., 2017. Phytosphingosine enhances moisture level in human skin barrier through stimulation of the filaggrin biosynthesis and degradation leading to NMF formation. Arch. Dermatol. Res 309 (10), 795–803. https://doi.org/10.1007/s00403-017-1782-8.

Danese, A., Patergnani, S., Bonora, M., Wieckowski, M.R., Previati, M., Giorgi, C., Pinton, P., 2017. Calcium regulates cell death in cancer: Roles of the mitochondria and mitochondria-associated membranes (MAMs). Biochim Biophys. Acta Bioenerg. 1858 (8), 615–627. https://doi.org/10.1016/j.bbabio.2017.01.003.

Fischer, C.L., Drake, D.R., Dawson, D.V., Blanchette, D.R., Brogden, K.A., Wertz, P.W., 2012. Antibacterial activity of sphingoid bases and fatty acids against Gram-positive and Gram-negative bacteria. Antimicrob. Agents Chemother. 56 (3), 1157–1161. https://doi.org/10.1128/aac.05151-11.

de la Fuente-Herreruela, D., Gónzalez-Charro, V., Almendro-Vedia, V.G., Morán, M., Martín, M.Á., Lillo, M.P., Natale, P., López-Montero, I., 2017. Rhodamine-based sensor for real-time imaging of mitochondrial ATP in living fibroblasts. Biochim Biophys. Acta Bioenerg. 1858 (12), 999–1006. https://doi.org/10.1016/j.bbabio.2017.09.004.

Fugio, L.B., Coeli-Lacchini, F.B., Leopoldino, A.M., 2020. Sphingolipids and mitochondrial dynamic. Cells 9 (3). https://doi.org/10.3390/cells9030581.

Genovese, I., Carinci, M., Modesti, L., Aguiari, G., Pinton, P., Giorgi, C., 2021. Mitochondria: insights into crucial features to overcome cancer chemoresistance. Int J. Mol. Sci. 22 (9), 4770. https://doi.org/10.3390/ijms22094770.

Ho, J.C., Michalak, A.M., Pahlevan, N., 2019. Widespread global increase in intense lake phytoplankton blooms since the 1980s. Nature 574 (7780), 667–670. https://doi.org/10.1038/s41586-019-1648-7.

Huisman, J., Codd, G.A., Paerl, H.W., Ibelings, B.W., Verspagen, J.M.H., Visser, P.M., 2018. Cyanobacterial blooms. Nat. Rev. Microbiol 16 (8), 471–483. https://doi.org/10.1038/s41579-018-0040-1.

Janssen, E.M., 2019. Cyanobacterial peptides beyond microcystins - a review on co-occurrence, toxicity, and challenges for risk assessment. Water Res 151, 488–499. https://doi.org/10.1016/j.watres.2018.12.048.

Jiayao, W., 2021. Effects of Microcystis aeruginosa exudates on mitochondrial structure and function in NCE-2 cells [D]. School of Ecology and Environmental Science. Yunnan University, Kunming, Yunnan, China, p. 5.

Jodeiri Farshbaf, M., Ghaedi, K., 2017. Huntington's disease and mitochondria. Neurotox. Res 32 (3), 518–529. https://doi.org/10.1007/s12640-017-9766-1.

Jones, M.R., Pinto, E., Torres, M.A., Dörr, F., Mazur-Marzec, H., Szubert, K., Tartaglione, L., Dell'Aversano, C., Miles, C.O., Beach, D.G., McCarron, P., Sivonen, K., Fewer, D.P., Jokela, J., Janssen, E.M., 2021. CyanoMetDB, a comprehensive public database of secondary metabolites from cyanobacteria. Water Res 196, 117017. https://doi.org/10.1016/j.watres.2021.117017.

Kondo, N., Ohno, Y., Yamagata, M., Obara, T., Seki, N., Kitamura, T., Naganuma, T., Kihara, A., 2014. Identification of the phytosphingosine metabolic pathway leading to odd-numbered fatty acids. Nature Communications 5. https://doi.org/10.1038/ncomms6338.

Kulikov, A.V., Luchkina, E.A., Gogvadze, V., Zhivotovsky, B., 2017. Mitophagy: link to cancer development and therapy. Biochem Biophys. Res Commun. 482 (3), 432–439. https://doi.org/10.1016/j.bbrc.2016.10.088.

Lee, J.S., Min, D.S., Park, C., Park, C.S., Cho, N.J., 2001. Phytosphingosine and C2-phytoceramide induce cell death and inhibit carbachol-stimulated phospholipase D activation in Chinese hamster ovary cells expressing the Caenorhabditis elegans muscarinic acetylcholine receptor. Febs Letters 499 (1-2). https://doi.org/10.1016/S0014-5793(01)02527-3.

Li, C., Qing, T., Rahman, M.K., Wu, F., 2020. Effect of anti-fungal compound phytosphingosine in wheat root exudates on the rhizosphere soil microbial community of watermelon. Plant Soil 456, 223–240. https://doi.org/10.1007/s11104-020-04702-1.

Lou, G., Palikaras, K., Lautrup, S., Scheibye-Knudsen, M., Tavernarakis, N., Fang, E.F., 2020. Mitophagy and Neuroprotection. Trends Mol. Med 26 (1), 8–20. https://doi.org/10.1016/j.molmed.2019.07.002.

Ly, J.D., Grubb, D.R., Lawen, A., 2003. The mitochondrial membrane potential (deltapsi (m)) in apoptosis; an update. Apoptosis 8 (2), 115–128. https://doi.org/10.1023/a:1022945107762.

Murphy, E., Steenbergen, C., 2020. Regulation of mitochondrial Ca2+ uptake. Annu Rev. Physiol. 83, 107–126. https://doi.org/10.1146/annurev-physiol-031920-092419.

Nagahara, Y., Shinomiya, T., Kuroda, S., Kaneko, N., Nishio, R., Ikekita, M., 2005. Phytosphingosine induced mitochondria-involved apoptosis. Cancer Sci. 96 (2), 83–92. https://doi.org/10.1111/j.1349-7006.2005.00012.x.

Ostaszewska-Bugajska, M., Podgórska, A., Szal, B., 2022. Markers for mitochondrial ROS status. Methods Mol. Biol. 2363, 199–213. https://doi.org/10.1007/978-1-0716-1653-6_15.

Paillard, M., Csordás, G., Huang, K.T., Várnai, P., Joseph, S.K., Hajnóczky, G., 2018. MICU1 interacts with the D-ring of the MCU pore to control Its Ca2+ flux and sensitivity to Ru360. Mol. Cell 72 (4), 778–785.e3. https://doi.org/10.1016/j.molcel.2018.09.008.

Park, J., An, G., Lim, W., Song, G., 2022. Dinitramine induces implantation failure by cell cycle arrest and mitochondrial dysfunction in porcine trophectoderm and luminal epithelial cells. J. Hazard Mater. 435, 128927 https://doi.org/10.1016/j.jhazmat.2022.128927.

Park, M.T., Choi, J.A., Kim, M.J., Um, H.D., Bae, S., Kang, C.M., Cho, C.K., Kang, S., Chung, H.Y., Lee, Y.S., Lee, S.J., 2003. Suppression of extracellular signal-related kinase and activation of p38 MAPK are two critical events leading to caspase-8- and mitochondria-mediated cell death in phytosphingosine-treated human cancer cells. J. Biol. Chem. 278 (50), 50624–50634. https://doi.org/10.1074/jbc.M309011200.

Pei, Y., Xu, R., Macisaac, H.J., Chang, X., 2019. Effects of cyanobacterial secondary metabolites on phytoplankton community succession. Phytochemistry 323–344. https://doi.org/10.1007/978-3-319-76887-8_12-1.

Rehberger, K., Kropf, C., Segner, H., 2018. In vitro or not in vitro: a short journey through a long history. Environ. Sci. Eur. 2018 30 (1), 23. https://doi.org/10.1186/s12302-018-0151-3.

Schofield, J.H., Schafer, Z.T., 2021. Mitochondrial reactive oxygen species and mitophagy: a complex and nuanced relationship. Antioxid. Redox Signal 34 (7), 517–530. https://doi.org/10.1089/ars.2020.8058.

Singh, A., Kukreti, R., Saso, L., Kukreti, S., 2019. Oxidative stress: a key modulator in neurodegenerative diseases. Molecules 24 (8), 1583. https://doi.org/10.3390/molecules24081583.

Song, X., Zhang, J., Wang, M., Liu, W., Gu, X., Lv, C., 2011. Astaxanthin induces mitochondria-mediated apoptosis in rat hepatocellular carcinoma CBRH-7919 cells. Biol. Pharm. Bull. 34 (6), 839–844. https://doi.org/10.1248/bpb.34.839.

Taha, T.A., Mullen, T.D., Obeid, L.M., 2006. A house divided: ceramide, sphingosine, and sphingosine-1-phosphate in programmed cell death. Biochim. Et. Biophys. Acta 1758 (12), 2027–2036. https://doi.org/10.1016/j.bbamem.2006.10.018.

Wang, C., Xie, N., Wang, Y., Li, Y., Ge, X., Wang, M., 2015. Role of the mitochondrial calcium uniporter in rat hippocampal neuronal death after pilocarpine-induced status epilepticus. Neurochem Res 40 (8), 1739–1746. https://doi.org/10.1007/s11064-015-1657-3.

Wang, L., Zi, J., Xu, R., Macisaac, H.J., Hou, X., Chang, X., 2017. Allelopathic effects of Microcystis aeruginosa on green algae and a diatom: evidence from exudates addition and co-culturing. Harmful Algae 61, 56–62. https://doi.org/10.1016/j.hal.2016.11.010.

Xu, R., Wu, F., Macisaac, H.J., Wu, C., Wang, X., Chang, X., 2015. Recovery limitation of endangered Ottelia acuminata by allelopathic interaction with cyanobacteria. Aquat. Ecol. 49 (3), 333–342. https://doi.org/10.1007/s10452-015-9528-1.

Xu, R., Macisaac, H.J., Pei, Y., Yin, L., Wang, X., Chang, X., 2016. Growth phase-dependent allelopathic effects of cyanobacterial exudates on *Potamogeton crispus* L. seedlings. Hydrobiologia 767 (1), 137–149. https://doi.org/10.1007/s10750-015-2489-5.

Xu, R., Jiang, Y., Macisaac, H.J., Chen, L., Li, J., Xu, J., Wang, T., Zi, Y., Chang, X., 2019. Blooming cyanobacteria alter water flea reproduction via exudates of estrogen analogues. Sci. Total Environ. 696, 133909 https://doi.org/10.1016/j.scitotenv.2019.133909.

Yang, S., Lian, G., 2020. ROS and diseases: role in metabolism and energy supply. Mol. Cell Biochem 467 (1–2), 1–12. https://doi.org/10.1007/s11010-019-03667-9.

Zhou, Y., Xu, J., Xu, R., Macisaac, H.J., McKay, M., Chang, X., 2022. Comparative metabolomic analysis of exudates of microcystin-producing and microcystin-free Microcystis aeruginosa strains. Front. Microbiol. Submitted for publication.

Zi, J., Pan, X., Macisaac, H.J., Yang, J., Chang, X., 2017. Cyanobacteria blooms induce embryonic heart failure in an endangered fish species. Aquat. Toxicol. 194, 78–85. https://doi.org/10.1016/j.aquatox.2017.11.007.